Optical Engineering 44(2), 025006 (February 2005)

# Design and fabrication of a dense wavelength division demultiplexer with grism structure

**Jyh-Rou Sze**
**Mao-Hong Lu,** MEMBER SPIE
National Chiao-Tung University
Department of Photonics and Institute of Electro-Optical Engineering
1001 Ta-Hsueh Road
Hsinchu 300, Taiwan
E-mail: sze.eo88g@nctu.edu.tw

**Abstract.** The implementation of a low-loss demultiplexer with a KRS-5 grism structure for a dense wavelength division demultiplexing (DWDDM) system in fiber communication is carried out. The system has 16 channels with wavelength spacing of 0.8 nm in the C-band wavelength region. This device is successfully fabricated by a precise plunge-cut diamond-turning technology. Numerical calculations and measurements indicate that this DWDDM is polarization independent and has higher optical efficiency and signal to noise ratio (SNR). © *2005 Society of Photo-Optical Instrumentation Engineers.* [DOI: 10.1117/1.1849195]

Subject terms: grism; dense wavelength division demultiplexer; plunge-cut diamond-turning technology.

Paper 040405R received Jun. 23, 2004; revised manuscript received Aug. 23, 2004; accepted for publication Aug. 23, 2004; published online Feb. 8, 2005.

## 1 Introduction

In recent years, it has become more and more important to develop a high-capacity and high-speed transmission system in the rapidly growing information industry. Dense wavelength division demultiplexing (DWDDM) systems provide a new dimension solving capacity and flexibility problems in the optical communication network. The key component in the DWDDM system is a wavelength demultiplexer.

To implement DWDDM, several devices and configurations have been proposed by many researchers.[1–12] Conventional filters made of dielectric thin films[2] and fiber Bragg gratings[3] would not seem suitable to perform as high-channel-count demultiplexers because they filter light in a serial manner and so must be used in combination with other technologies such as interleavers and circulators, which may cause high insertion loss and increase system costs. With advances in waveguide photonic integrated circuits, demultiplexers based on planar arrayed waveguide gratings (AWGs)[4] have potential use in DWDDM networks. These devices process optical signals in a parallel manner, which is preferred for high-channel-capacity networks. Yet their promise of large-volume manufacture abilities is hindered by typically low yields and poor performance, including high insertion loss, polarization sensitivity, small free-spectral range, and lack of temperature stabilization. They may be used in combination with other technologies such as thermal compensators[6] and polarization converters,[7] which may cause high insertion loss and system costs. For monodirectional or bidirectional links, optical gratings provide the lowest crosstalk and the largest number of channels. Several papers[8–12] have reported the design and manufacture of demultiplexers by using reflection diffraction gratings or concave gratings.

An optical element called a grism, consisting of a transmission grating and a prism, is often used in several applications,[13–19] i.e., astronomical spectrographs, spectrometers, and so on. In this work, we use the grism instead of reflection gratings in the DWDDM system. The designed DWDDM system is shown in Fig. 1(a). The major advantages of using transmitting grisms are: 1. a relatively large tolerance for optical alignment, and 2. the ability of reducing the channel spacing to 0.4 nm or less by putting the same grisms in a series, as shown in Fig. 1(b). When the incident beam passes through two grisms in a series, it makes double diffractions. This configuration would increase the resolving power of the DWDDM system by double. The first advantage is usually realized by designing the system as a direct transmitting optics, where one puts a grism in the optical path with its prism vertex angle adjusted to make the specific order diffraction beam straight along the optical axis at a reference wavelength. If the tilt angle of the grism is $\delta\alpha_1$, the deviation of the incident angle for the transmitting grism is $\delta\alpha_2 = \delta\alpha_1 \cos(\alpha_1)/n_s \cos(\alpha_2)$, where $n_s$ is the refraction index of the grism substrate, as shown in Fig. 2. The angle $\delta\alpha_2$ would be smaller than $\delta\alpha_1$ for the grism. Under the same condition, the deviation angle $\delta\alpha_2$ equals $\delta\alpha_1$ for the reflection grating. The tilt tolerance of the transmitting grism would be larger than the reflection grating.

The grism should be considered to have high optical efficiency, and to be fabricated and replicated easily. There are several methods for fabricating a blazed grism, which has high diffraction efficiency. The most popular method of making a grism is the resin replication of a blazed diffraction grating on a high index prism surface.[19] However, most resins have some absorption at infrared wavelengths. Other possible approaches are direct ruling of grooves[20] or oblique ion-beam etching[21] on a high refractive index substrate. The grism made of high-index material can diffract the beam in the high order with a small vertex angle, which gives a large angular dispersion. However, most optical glasses and crystalline materials are too hard to be processed by a ruling engine.

KRS-5 (ISP Optics Corporation) is an infrared material with high refractive index and is transparent in the C band.

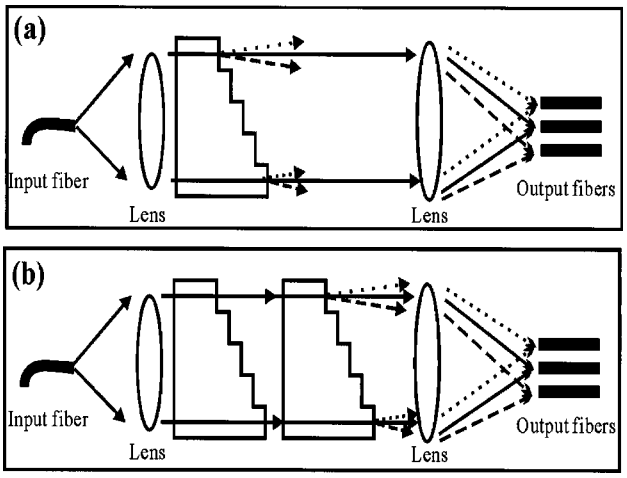


**Fig. 1** Schematic diagram of a demultiplexer using the grism: (a) demultiplexing mode and (b) series mode.

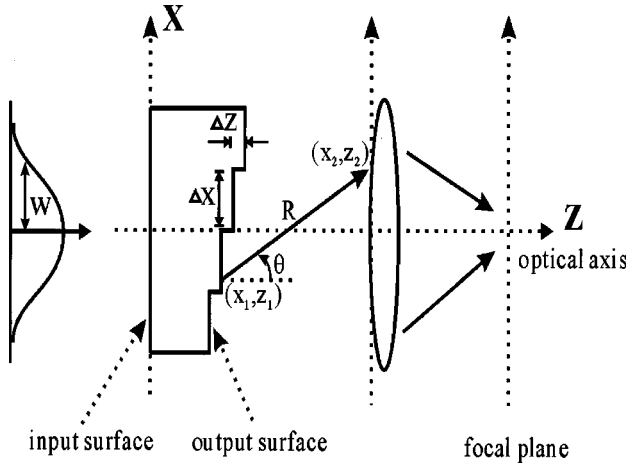


**Fig. 3** Schematic representation of a DWDDM.

It has a low melting point of 414.5 °C, low hardness, and could be easily fabricated by using the plunge-cut diamond turning technology and also replicated with conventional embossing techniques. For the prior reasons we chose KRS-5 to make the grism, which could be used for mass production in the future, and make DWDDMs cost less.

In this study, we try to determine whether the grism structure has a desired performance for DWDDM applications.

## 2 Calculation Method

As shown in Fig. 1(a), the DWDDM comprises one collimator lens, one grism, and one focal lens. In this work, the 16 channels with a wavelength spacing of 0.8 nm in the C band are designed.

Assuming the surrounding material of this element is air, the angles of light rays given counterclockwise are positive, and those are negative else. The grating equation can be written as

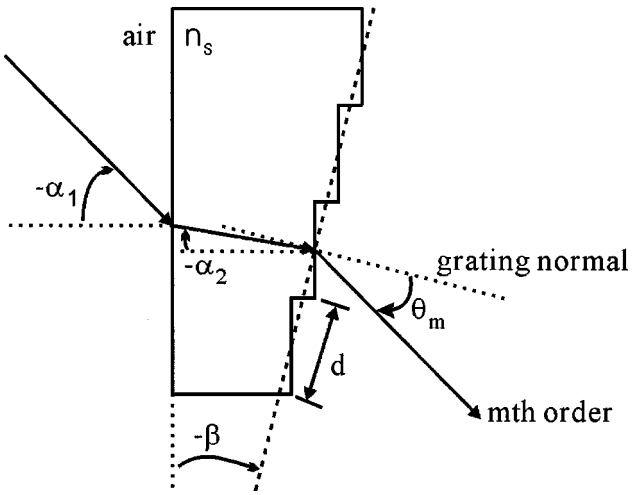


**Fig. 2** Schematic representation of a grism.

$$\sin(\theta_m)-n_s(\lambda_f)\sin(\beta-\alpha_2)=m\frac{\lambda_f}{d}. \quad (1)$$

Here $m$ is the diffraction order and $d$ is the period of grating. The $\theta_m$ is the $m$'th order diffraction angle measured from the normal to the grating, and the $\beta$ is the blazed angle of grating, as shown in Fig. 2. $n_s(\lambda_f)$ is the refractive index of KRS-5 material at the reference wavelength $\lambda_f$ and could be expressed by the following dispersion formula,

$$n_s^2(\lambda)=a_0+a_1\lambda^2+a_2\lambda^{-2}+a_3\lambda^{-4}+a_4\lambda^{-6}+a_5\lambda^{-8}, \quad (2)$$

where $a_0=5.66699$, $a_1=-0.00048$, $a_2=-0.02409$, $a_3=2.18849$, $a_4=-2.44416$, and $a_5=0.61575$.

Under the on-blaze condition ($\theta_m=\beta-\alpha_1$), the grating should have maximum efficiency in the $m$'th order at the wavelength $\lambda_f$. From Eq. (1) the blazed angle is given by

$$\sin\beta=\frac{m\lambda_f}{[\cos\alpha_1-n_s(\lambda_f)\cos\alpha_2]d}, \quad (3)$$

where $\alpha_1$ is the input angle of the beam incident on the grism. The blazed grating has a period $d=12\,\mu$m that is about eight times larger than the reference wavelength $\lambda_f=1550.8$ nm. In this case, the grating is polarization independent and the scalar diffraction theory is available. Within the limitations of the fabrication machine used in this work, the ninth diffraction order and 400 grooves are chosen. If both angles $\alpha_1$ and $\alpha_2$ equal zero, the blazed angle $\beta$ is 54.75 deg. A multiple-wavelength Gaussian beam with a divergence angle of $6.13\times10^{-3}$ deg and Gaussian beam parameter $w=2.3$ mm is normally incident on the input surface of the grism, as shown in Fig. 3. Behind the grism, a lens with focal length of 29.47 mm is used.

To verify our design of the grism structure, the field distributions behind the grism are calculated with the Huygens-Fresnel principle[22] and given by

$$E_2(x_2,\lambda)=A\sum_{p=1}^{N_1}\frac{\exp(-i\pi/4)}{\sqrt{\lambda}}\int_{[(p-1)-N_1/2]\Delta x}^{[p-N_1/2]\Delta x}\frac{\cos(\theta/2)}{\sqrt{R}}\times\exp\{ik[R+p\Delta z n_s(\lambda)]\}\exp\left[-\left(\frac{x_1}{w}\right)^2\right]dx_1. \tag{4}$$

Here, $A$ is a constant, and $\theta$ is the angle of wave vector $k$ to the grating facet normal. $N_1$ is the total number of grooves. $\Delta x$ and $\Delta z$ are the width and depth of the groove, respectively, and they are determined by $\Delta x=d\cos\beta$ and $\Delta z=d\sin\beta$. The $R$ is the distance from $(x_1,z_1)$ to $(x_2,z_2)$, as shown in Fig. 3. The diffraction field from the output surface of the grism passes through the focal lens, and focuses on the focal plane.

The amplitude distribution of the incident Gaussian beam could be described by

$$u_0(x)=\exp\left[-\left(\frac{x}{w}\right)^2\right]=\int_{-\infty}^{\infty}[\sqrt{\pi}w\exp(-\pi^2w^2\varsigma^2)]\exp(i2\pi\varsigma x)d\varsigma. \tag{5}$$

Neglecting reflection and transmission losses, the transmission function of the grism could be written as

$$g(x,\lambda)=\frac{1}{N_1\Delta x}\sum_{p=1}^{N_1}\exp[-i\phi(\lambda,p)]\times\mathrm{rect}\left[\frac{x-p\Delta x+N_1\Delta x/2}{\Delta x}\right], \tag{6}$$

where $\phi(\lambda,p)$ is the phase function of the grism, given by

$$\phi(\lambda,p)=\frac{2\pi}{\lambda}[n_s(\lambda)-1.0]p\Delta z. \tag{7}$$

Under the blazed condition, $\phi(\lambda,p)$ equals $2\pi m_0 p$ at $\lambda=\lambda_f$, and Eq. (6) could be rewritten as follows,

$$\phi(\lambda,p)=2\pi\left[\frac{\lambda_f}{n_f-1}\frac{n_s(\lambda)-1}{\lambda}\right]m_0p. \tag{8}$$

Here $m_0$ is the designed diffraction order of the grism. A Gaussian beam normally illuminates the grism, and the field distribution behind the grism equals $u(x,\lambda)=u_0(x)g(x,\lambda)$. In the Kirchholff approximation, the Fourier transform of $u(x,\lambda)$ is

$$\begin{aligned}U(\xi,\lambda)&=\int_{-\infty}^{\infty}u(x,\lambda)\exp(-i2\pi\xi x)dx\\&=\int_{-\infty}^{\infty}\exp[i\pi N_1(\xi-\varsigma)\Delta x]\mathrm{sinc}[(\xi-\varsigma)\Delta x]\times[\sqrt{\pi}w\exp(-\pi^2w^2\varsigma^2)]\frac{1}{N_1}\\&\quad\times\sum_{p=1}^{N_1}\exp\left(-i2\pi\left\{\left[\frac{\lambda_f}{n_f-1}\frac{n_s(\lambda)-1}{\lambda}\right]m_0+(\xi-\varsigma)\Delta x\right\}p\right)d\varsigma\\&=\int_{-\infty}^{\infty}\exp[i\pi N_1(\xi-\varsigma)\Delta x]\mathrm{sinc}[(\xi-\varsigma)\Delta x]\times[\sqrt{\pi}w\exp(-\pi^2w^2\varsigma^2)]\frac{1}{N_1}\\&\quad\times\sum_{p=1}^{N_1}\exp(-i2\pi mp)d\varsigma,\end{aligned} \tag{9}$$

where

$$m=\left[\frac{\lambda_f}{n_f-1}\frac{n_s(\lambda)-1}{\lambda}\right]m_0+(\xi-\varsigma)\Delta x. \tag{10}$$

In Eq. (9), the summation vanishes, except that the following condition is satisfied:

$$\sum_{p=1}^{N_1}\exp(-i2\pi mp)=\begin{cases}N_1, & m=\text{integer}\\0, & \text{otherwise}\end{cases}. \tag{11}$$

If $m$ equals an integer, the intensity of the $m$'th order diffraction light at wavelength $\lambda$ could be given by

$$|U(m,\lambda)|^2=\left|\int_{-\infty}^{\infty}\exp\left(i\pi N_1\left\{m-\left[\frac{\lambda_f}{n_f-1}\frac{n_s(\lambda)-1}{\lambda}\right]m_0\right\}\right)\times\mathrm{sinc}\left\{m-\left[\frac{\lambda_f}{n_f-1}\frac{n_s(\lambda)-1}{\lambda}\right]m_0\right\}\times\sqrt{\pi}w\exp[-\pi^2w^2\varsigma^2]d\varsigma\right|^2, \tag{12}$$

where the factor $\sqrt{\pi}w\exp[-\pi^2w^2\varsigma^2]$ represents the spatial divergence of diffraction beams. In this work, since the incident Gaussian beam has a large beam waist $w=2.3$ mm, the contribution of the factor is only from a very small value $\varsigma$, which has a negligible influence on the other functions in the integral of Eq. (12). The other functions in the integral can be considered to be independent of $\varsigma$, and we have

$$|U(m,\lambda)|^2=\left(\mathrm{sinc}\left\{m-\left[\frac{\lambda_f}{n_f-1}\frac{n_s(\lambda)-1}{\lambda}\right]m_0\right\}\right)^2. \tag{13}$$

The $m$'th order diffraction efficiency of the grism is defined as

$$\eta(m,\lambda)=\frac{|U(m,\lambda)|^2}{\Sigma_{m'}|U(m',\lambda)|^2}. \tag{14}$$

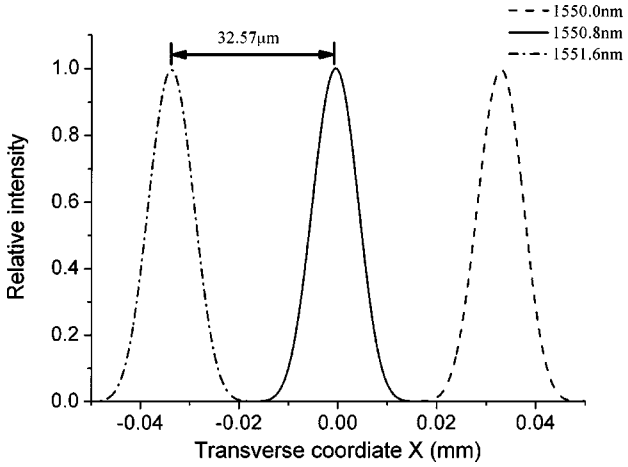


**Fig. 4** A part of the calculated transverse intensity distributions on the focal plane.

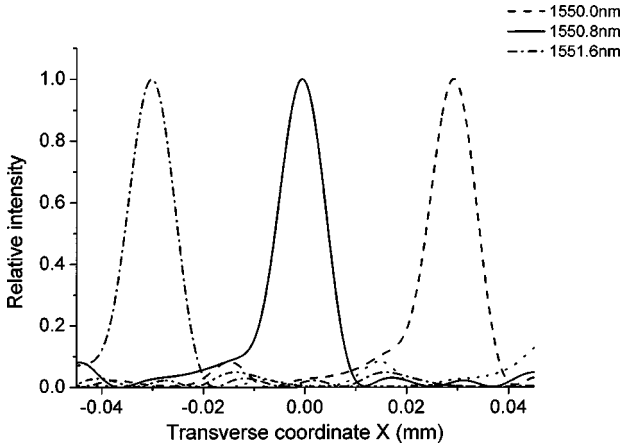


**Fig. 6** A part of the calculated transverse intensity distributions with variance values $\delta_x = \delta_z = 0.05\ \mu$m.

The total optical crosstalk in channel $j$ is defined by the signal-to-noise ratio (SNR),

$$\mathrm{SNR}_j = \frac{\Phi_{jj}}{\Sigma_{i \neq j} \Phi_{ij}}, \tag{15}$$

where $\Phi_{ij}$ indicates the crosstalk power in channel $j$ of wavelength $\lambda_j$ from other channels, and $\Phi_{jj}$ is the output power of wavelength $\lambda_j$ in channel $j$.

The influences of fabrication errors on the optical performance are evaluated by using the deviation probability function. We assume that the deviation of grating width $\Delta x$ and depth $\Delta z$ is independent, and the deviation values could be described by the Gaussian random probability distributions,[23]

$$f_G(\delta_{x,j}) = \frac{1}{(2\pi\sigma_x^2)^{1/2}} \exp[-(\delta_{x,j} - a_x)^2 / 2\sigma_x^2], \tag{16}$$

$$f_G(\delta_{z,j}) = \frac{1}{(2\pi\sigma_z^2)^{1/2}} \exp[-(\delta_{z,j} - a_z)^2 / 2\sigma_z^2],$$
$$j = 1,2,...,N_2, \tag{17}$$

where $\delta_{x,j}(\delta_{z,j})$, $a_x(a_z)$, and $\sigma_x(\sigma_z)$ represent the deviation value, mean value, and variance value of the grating width (depth), respectively. The suffix $j$ denotes the $j$'th grating groove. The new width $\Delta x + \delta_{x,j}$ and depth $\Delta z + \delta_{z,j}$ for each groove are given by Eqs. (16) and (17), respectively. The field distributions with fabrication errors are obtained by substituting them into Eq. (4).

## 3 Calculation Results

The intensity distributions as a function of position on the focal plane are shown in Fig. 4, where the spatial separation between two adjacent channels, corresponding to the wavelength spacing of 0.8 nm, is 32.57 $\mu$m and the waist spot size of the focal Gaussian beam at the reference wavelength is about 20.9 $\mu$m. The transmission spectra of the designed DWDDM as a function of wavelength for 16 channels are

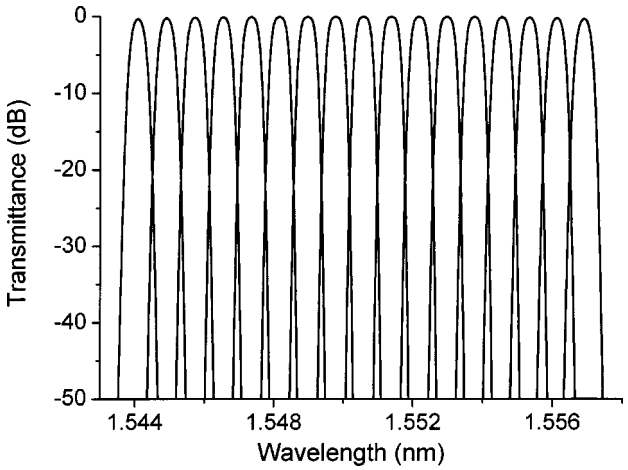


**Fig. 5** Calculated transmission spectra of the designed DWDDM.

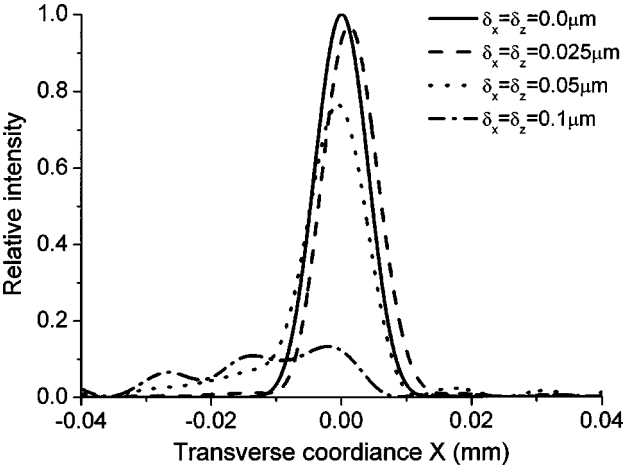


**Fig. 7** Calculated transverse intensity distributions at reference wavelength $\lambda_f = 1550.8$ nm with different variance values.

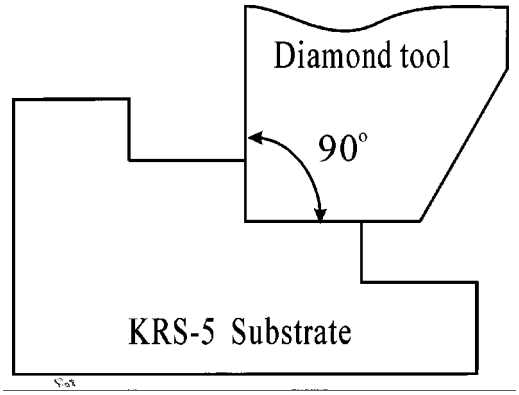


**Fig. 8** Cross-section view of plunge-cut diamond-turning configuration.

shown in Fig. 5, where we can see that the designed demultiplexer has high optical efficiency and signal-to-noise ratio, and the full width at half maximum (FWHM) of each channel spectrum is 0.678 nm, which is smaller than the requirement 0.8 nm. We calculated and analyzed the influences of fabrication errors on the optical performance. In this calculation, we assume that both mean values $a_x$ and $a_z$ are zero, and both variance values $\delta_x$ and $\delta_z$ are 0.05 $\mu$m. With the deviation values given by Eqs. (16) and (17), the intensity distributions at the central wavelength of each channel were calculated, and a part of the results are shown in Fig. 6. The intensity distributions at reference wavelengths with different variance values are shown in Fig. 7 for comparison.

## 4 Experimental Results

The blazed grating was fabricated directly on the hypotenuse of a KRS-5 prism by using plunge-cut diamond turning technology[24] (Machi NCAU-300E). This technology overcomes much of the turning mark problem[24] by cutting with the edge of the diamond tool, as shown in Fig. 8. A photograph of the fabricated grism is shown in Fig. 9. Figure 10 exhibits a part of the profile of the surface relief profile for the fabricated grating, measured with an optical profilemeter (Zygo New View 5000). Table 1 lists the profile errors of gratings produced in the making process. To check the performance of the fabricated grism, we measured the intensity distributions on the focal plane. Table 2

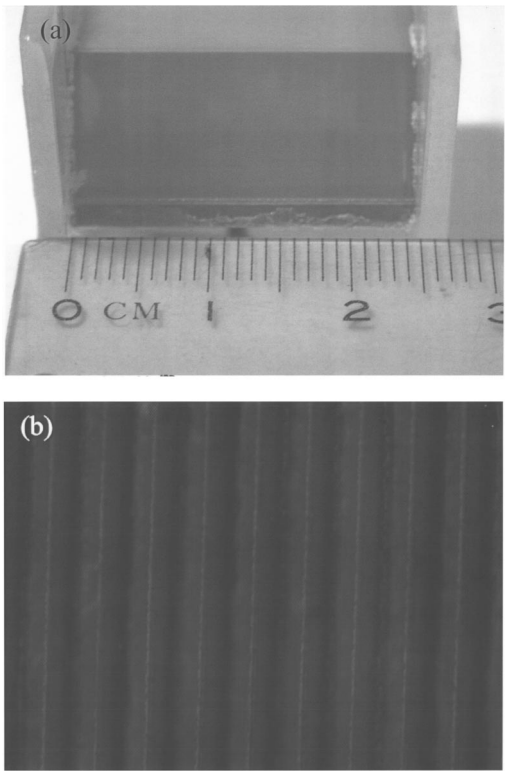


**Fig. 9** Photographs of fabricated grating: (a) real sample and (b) a part of the enlarged grating.

lists the calculated and measured optical loss for each component. Those losses are caused by reflection that can be reduced by the antireflection coating on the input and output surfaces.

The experimental setup for measuring the spot size and relative position of each channel wavelength is shown in Fig. 11. The incident beam with a bandwidth of 0.2 nm was provided by a tunable laser source (Anritsu MG9541A). An infrared charge-coupled device (CCD) camera (Electrophysic 7290A) with 20× objective was placed on the focal plane to record the output image for discrete wavelengths with wavelength separation of 0.8 nm. The intensity distribution at the reference wavelength is shown in Fig. 12. In this case, the light at the reference wavelength propagates along the optical axis and does not deflect by the grism. Its

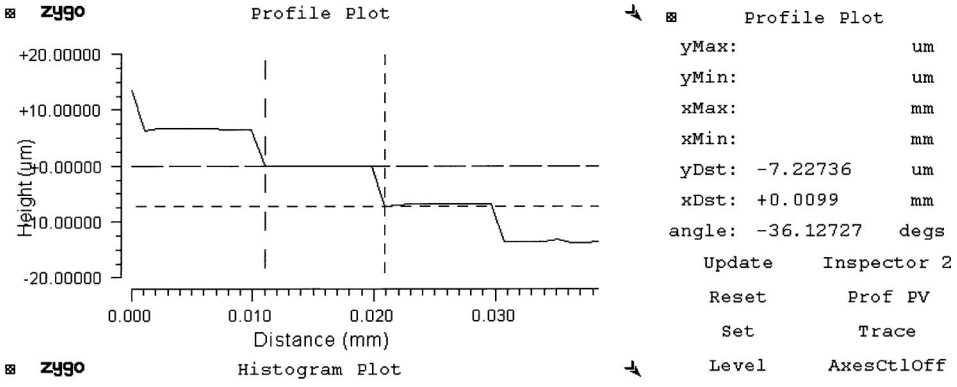


**Fig. 10** Section profile of surface relief of grating measured with the Zygo profilemeter.

**Table 1** Comparisons between designed and measured depth and width of grating.

| | Designed | Measured | Error |
|---|---|---|---|
| Depth of grating $\Delta z$ | 9.8 | 9.7 $\pm$0.4 | 1.02% |
| Width of grating $\Delta x$ | 6.93 | 6.78$\pm$0.3 | 2.26% |

**Table 2** Comparisons between calculated and measured optical transmittance of each component.

| | Calculated | Measured |
|---|---|---|
| Collimator lens | 0.99 | 0.96 |
| Grism | 0.684 | 0.672 |
| Focal lens | 0.926 | 0.903 |

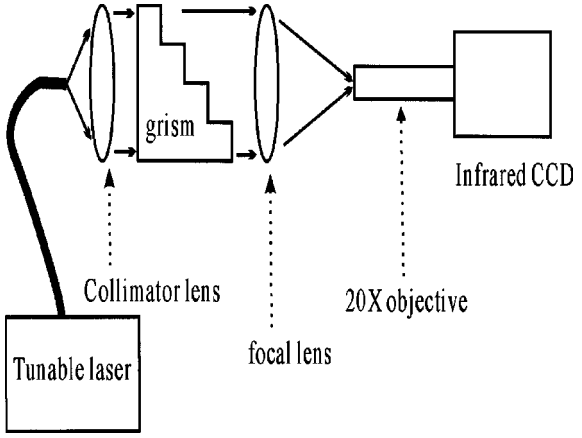


**Fig. 11** Experimental setup for measuring the spot size and relative position of each wavelength on the focal plane.

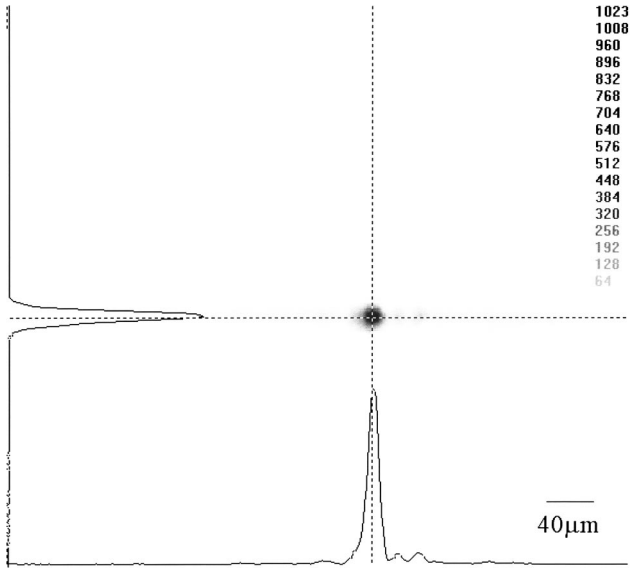


**Fig. 12** Measured intensity distribution at reference wavelength $\lambda_f$ = 1550.8 nm on the focal plane.

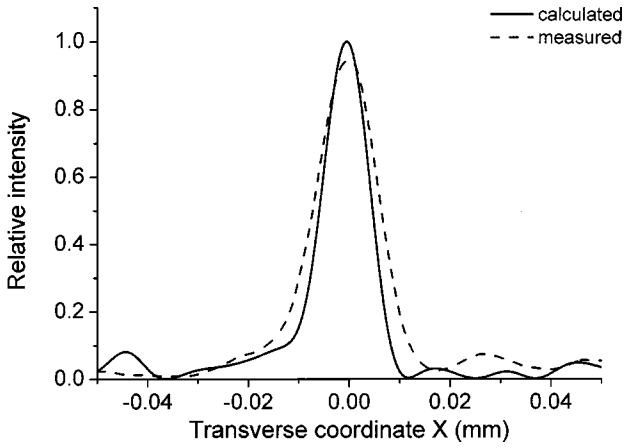


**Fig. 13** Comparison between the calculated and measured transverse intensity distributions on the focal plane at the reference wavelength $\lambda_f$ = 1550.8 nm.

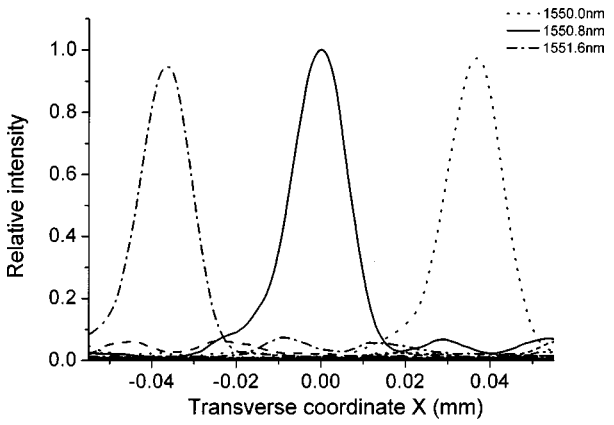


**Fig. 14** A part of the measured transverse intensity distributions on the focal plane.

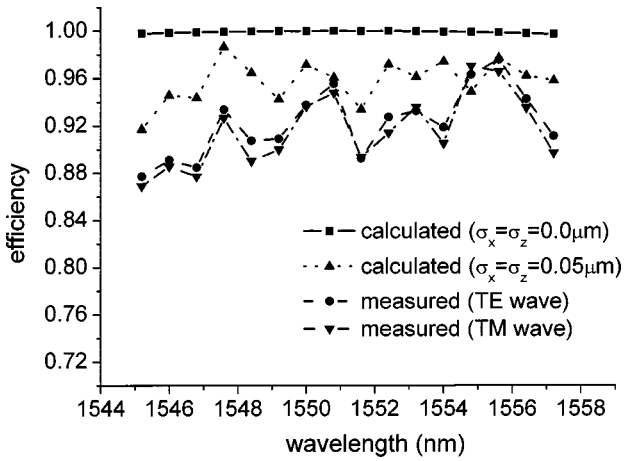


**Fig. 15** Comparison between the calculated and measured diffraction efficiency of the grism for each channel wavelength.

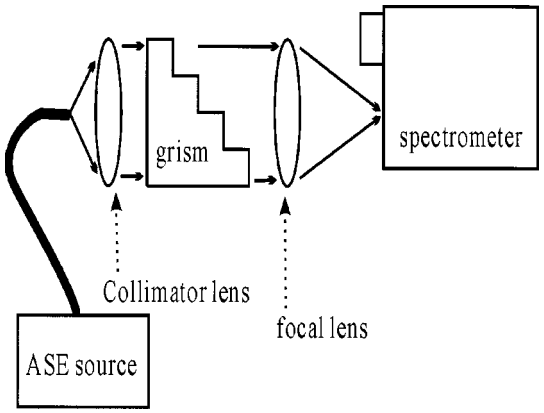


**Fig. 16** Experimental setup for measuring the transmission spectra of each channel.

spot is about circular symmetry, but there are a few stray spots in the transverse direction. This could be due to the turning errors of the grating and the residues in the ravine of the grating groove. To verify this point, we compare this result to that calculated with grating groove errors corresponding to the variance value $\delta_x = \delta_z = 0.05\ \mu$m, as shown in Fig. 13, where some small side peaks can be found. A part of the measured transverse intensity distributions are drawn in Fig. 14. The spot size and the spot separation between two adjacent channels are about 21.3 and 36.27 $\mu$m, respectively. The optical diffraction efficiency of the grism for each wavelength channel corresponding to an inner area of 24 $\mu$m diam was measured. The results are compared with the calculated, as shown in Fig. 15. The setup for measuring the transmission spectra of each channel is shown in Fig. 16. The incident beam with broad spectral band (1520 to 1570 nm) was provided by the amplified spontaneous emission (ASE) light source (Unice NA0101), and the transmission spectra for each channel were recorded by a spectrometer (Jobin Yvon Triax 550). The measured transmission spectra of 16 channels are demonstrated in Fig. 17, where the spectral passband of each channel at the FWHM is about 0.7 nm. The comparison

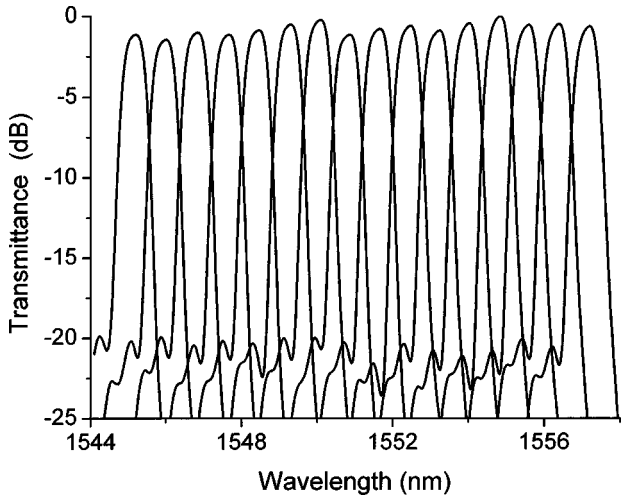


**Fig. 17** Measured transmission spectra of the fabricated DWDDM.

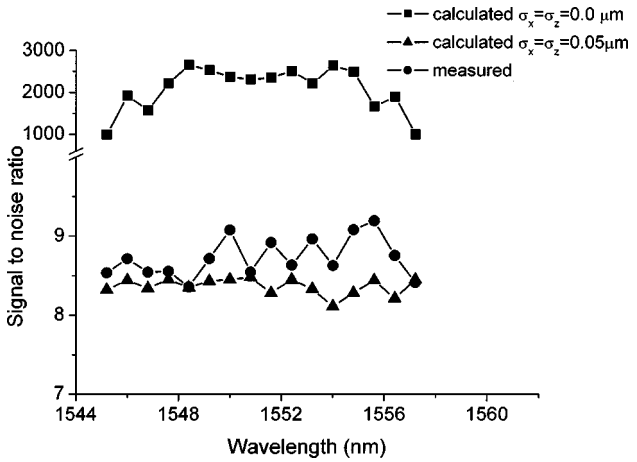


**Fig. 18** Comparison of the measured SNR with the calculated SNRs that correspond to a perfect grating ($\delta_x = \delta_z = 0.0\ \mu$m) and an imperfect grating ($\delta_x = \delta_z = 0.05\ \mu$m).

between the calculated and measured signal-to-noise ratio is shown in Fig. 18. The difference between the calculated and the measured should be mainly caused by the imperfections of the grating, such as deviation of the groove profile, pitch irregularity, etc. The calculation with variance value ($\delta_x = \delta_z = 0.05\ \mu$m) verifies this point, as shown in Fig. 18.

## 5 Conclusion

A KRS-5 grism is used to design and fabricate a low-loss demultiplexer for a DWDDM system. The performance of this demultiplexer is also calculated with the Huygens-Fresnel principle. The influences of fabrication errors on the optical performance are analyzed. The KRS-5 grism is successfully fabricated by precise plunge-cut diamond-turning technology. Numerical calculations and experimental measurements demonstrate that both agree very well. The demultiplexer has 16 channels with a wavelength spacing of 0.8 nm in the C band. Furthermore, narrower wavelength spacing could be obtained by using the same grisms in a series without redesigning the system.

### *Acknowledgments*

The authors gratefully acknowledge the National Science Council of the Republic of China for financial support of this research under project number NSC 92-2215-E-009-051, and the Precision Instrument Development Center for providing the measurement equipment. The grism was fabricated by the Mechanical Industry Research Laboratories of the Industrial Technology Research Institute.

### *References*

1. A. Othonos, J. Bismuth, M. Sweeny, A. P. Kevorkian, and J. M. Xu, "Superimposed grating wavelength division multiplexing in Ge-doped SiO2 Si planar waveguides," *Opt. Eng.* **37**(2), 717–720 (1998).
2. A. Michael and S. Cobey, "Optical multiplexing device," U.S. Patent No. 5,583,683 (1996).
3. F. Bilodeau, D. C. Johnson, S. Theriault, B. Malo, J. Albert, and K. O. Hill, "An all fiber dense wavelength division multiplexer/demultiplexer using photoimprinted Bragg gratings," *IEEE Photonics Technol. Lett.* **7**(4), 388 (1995).
4. J. F. Viens, C. L. Callender, J. P. Noad, L. A. Eldada, and R. A. Norwood, "Polymer-based waveguide devices for WDM applications," *Proc. SPIE* **3799**, 202–213 (1999).

5. V. Minier, A. Kevorkian, and J. M. Xu, ''Superimposed phase gratings in planar optical waveguides for wavelength demultiplexing applications,'' *IEEE Photonics Technol. Lett.* **5**, 330–333 (1993).
6. N. Ooba, Y. Hibino, Y. Inoue, and A. Sugita, ''Althermal silica-based arrayed-waveguide grating multiplexer using bimetal plate temperature compensator,'' *Electron. Lett.* **36**(21), 1800–1801 (2000).
7. Y. Inoue, Y. Ohmori, M. Kawachi, S. Ando, T. Sawada, and H. Takahashi, ''Polarization mode converter with polyimide half waveplate in silica-base planar lightwave circuits,'' *IEEE Photonics Technol. Lett.* **6**(5), 626–628 (1994).
8. M. Kajita, K. Kasahara, T. J. Kim, D. T. Neilson, I. Ogura, I. Redmond, and E. Schenfeld, ''Wavelength-division multiplexing free-space optical interconnect networks for massively parallel processing systems,'' *Appl. Opt.* **37**(18), 3746–3755 (1998).
9. K. I. Aoyama and J. I. Minowa, ''Low-loss optical demultiplexer for WDM systems in the 0.8 micrometer wavelength region,'' *Appl. Opt.* **18**(16), 2834–2836 (1979).
10. W. J. Tomlinson, ''Wavelength multiplexing in multimode optical fibers,'' *Electron. Lett.* **16**(8), 2180–2194 (1977).
11. B. D. Metcalf and J. F. Providakes, ''High-capacity wavelength demultiplexer with a large-diameter grin rod lens,'' *Appl. Opt.* **21**(5), 794–796 (1982).
12. M. Seki et al., ''20-channel micro-optic grating demultiplexer for 1.1–1.6 micrometer band using a small focusing parameter graded-index rod lens,'' *Electron. Lett.* **18**(6), 257–258 (1982).
13. N. Ebizuka, M. Lye, and T. Sasaki, ''Optically anisotropic crystalline grisms for astronomical spectrographs,'' *Appl. Opt.* **37**(7), 1236–1242 (1998).
14. W. A. Traub, ''Constant-dispersion grism spectrometer for channeled spectra,'' *J. Opt. Soc. Am. A* **7**(9), 1779 (1990).
15. S. Kane and J. Squier, ''Grism-pair stretcher compressor system for simultaneous second- and third-order dispersion compensation in chirped-pulse amplification,'' *J. Opt. Soc. Am. B* **14**(3), 661 (1997).
16. B. A. Richman, S. E. Bisson, R. Trebino, M. G. Mitchell, E. Sidick, and A. Jacobson, ''Achromatic phase matching for tunable second-harmonic generation by use of a grism,'' *Opt. Lett.* **22**(16), 1223–1225 (1997).
17. C. Pitris, B. E. Bouma, M. Shiskov, and G. J. Tearney, ''A grism-based probe for spectrally encoded confocal microscopy,'' *Opt. Exp.* **11**(2), 120–124 (2003).
18. N. Ebizuka, K. Oka, A. Yamada, M. Watanabe, K. Shimizu, K. Kodate, M. Kawabata, T. Teranishi, K. S. Kawabata, and M. Iye, ''Development of volume phase holographic (VPH) grism for visible to near infrared instruments of the 8.2 m Subaru telescope,'' *Proc. SPIE* **4842**, 319–328 (2003).
19. W. A. Rense, ''Techniques for rocket socket solar UV and for UV spectroscopy,'' *Space Sci. Rev.* **9**, 234–264 (1966).
20. L. Weitzel, A. Krabbe, H. Kroker, N. Thatte, L. E. Tacconi-Garman, M. Cameron, and R. Genzel, ''3D: The next generation near-infrared imaging spectrometer,'' *Astron. Astrophys., Suppl. Ser.* **119**, 531–546 (1996).
21. Y. Aoyagi and S. Namba, ''Blazed ion-etched holographic gratings,'' *Opt. Acta* **23**, 701–707 (1976).
22. S. Nonogaki, ''A rigorous solution of two-dimensional diffraction based on the Huygens-Fresnel principle,'' *Jpn. J. Appl. Phys., Part 1* **28**(5), 786–790 (1989).
23. W. H. Press, S. A. Teukolsky, W. T. Vetterling, and B. P. Flannery, *Numerical Recipes in Fortran*, 2nd ed., pp. 279–280, Cambridge, Univ. Press, Boston, MA (1992).
24. M. B. Fleming and M. C. Hutley, ''Blazed diffractive optics,'' *Appl. Opt.* **36**(20), 4635–4643 (1997).

**Jyh-Rou Sze** received his BS degree from the Department of Electrical Engineering at Private Chinese-Culture University in 1997 and MS degree from the Department of Electro-Optical Engineering at National Chiao-Tung University in 1999, where he is currently working toward his PhD. His current interests include the numerical methods applied to designing diffractive optical elements that have particular functions and fabricating the designed elements.

**Mao-Hong Lu** graduated from the Department of Physics at Fudan University in 1962. He then worked as a research staff member at the Shanghai Institute of Physics and Technology, Chinese Academy of Sciences, from 1962 to 1970, and the Shanghai Institute of Laser Technology from 1970 to 1980. He studied at the University of Arizona as a visiting scholar from 1980 to 1982. He is currently a professor at the Institute of Electro-Optical Engineering, National Chiao-Tung University.